Inhibition of Geranylgeranyl Diphosphate Synthase by Bisphosphonates and Diphosphates: A Potential Route to New Bone Antiresorption and Antiparasitic Agents

Christina M. Szabo,[†] Yoshihiro Matsumura,[‡] Sayaka Fukura,[‡] Michael B. Martin,[†] John M. Sanders,[†] Suraj Sengupta,[†] John A. Cieslak,[†] Timothy C. Loftus,[†] Christopher R. Lea,[†] Hyung-Jae Lee,[†] Ali Koohang,[†] Robert M. Coates,[†] Hiroshi Sagami,[‡] and Eric Oldfield*[,†]

Department of Chemistry, University of Illinois at Urbana−Champaign, 600 South Mathews Avenue, Urbana, Illinois 61801, and Institute of Multidisciplinary Research for Advanced Materials, Tohoku University, Katahira 2-1-1, Aoba-ku, Sendai 980-8577, Japan

Received January 1, 2002

We report the inhibition of a human recombinant geranylgeranyl diphosphate synthase (GGPPSase) by 23 bisphosphonates and six azaprenyl diphosphates. The IC_{50} values range from 140 nM to 690 μM. None of the nitrogen-containing bisphosphonates that inhibit farnesyl diphosphate synthase were effective in inhibiting the GGPPSase enzyme. Using three-dimensional quantitative structure−activity relationship/comparative molecular field analysis (CoMFA) methods, we find a good correlation between experimental and predicted activity: $R^2 = 0.938$, $R_{cv}^2 = 0.900$, $R_{bs}^2 = 0.938$, and F-test = 86.8. To test the predictive utility of the CoMFA approach, we used three training sets of 25 compounds each to generate models to predict three test sets of three compounds. The rms pIC_{50} error for the nine predictions was 0.39. We also investigated the pharmacophore of these GGPPSase inhibitors using the Catalyst method. The results demonstrated that Catalyst predicted the pIC_{50} values for the nine test set compounds with an rms error of 0.28 (R^2 between experimental and predicted activity of 0.948).

Introduction

The isoprenoid biosynthetic pathway is a key target for chemotherapeutic intervention in a number of diseases. For example, the statins are an important class of inhibitors of the enzyme hydroxymethylglutaryl coenzyme A reductase (HMGCoA-R) and drugs such as Lipitor, Zocor, and Pravachol are used extensively as cholesterol-lowering agents.[1] A second class of inhibitors consists of the nitrogen-containing bisphosphonates, such as pamidronate (Aredia, **36**), alendronate (Fosamax, **35**), and risedronate (Actonel, **27**), used in treating bone resorption diseases. These compounds are thought to act as aza-carbocation reactive intermediate analogues of prenyl carbocation intermediates,[2] and they have recently been shown to inhibit farnesyl diphosphate synthase (FPPSase).[3−7] A reduction in farnesyl diphosphate (FPP) levels results in decreases in geranylgeranyl diphosphate (GGPP) concentrations since GGPP is formed from FPP by geranylgeranyl diphosphate synthase (GGPPSase). This effectively blocks protein geranylgeranylation and appears to lead to apoptotic programmed cell death (PCD) at high concentrations[8] and to ultrastructural changes at lower concentrations.[9] The IC_{50} (K_i) values for some of the bisphosphonates, such as pamidronate, are quite high (~0.5 μM), but elevated local levels in the target cells, osteoclasts, are thought to be present due to the specific adsorption of the bisphosphonates onto the calcium hydroxyapatite surfaces of bone. A third class of isoprene (terpene) biosynthesis inhibitors act further downstream of FPPSase and directly block sterol formation. Examples are squalene synthase inhibitors, squalene monooxygenase inhibitors (e.g., terbinafine), and the azole inhibitors (e.g., fluconazole, a cytochrome P_{450} 14-α demethylase inhibitor). Compounds such as terbinafine and the azoles are important antifungal agents, which inhibit the formation of the essential sterol, ergosterol. Moreover, they have activity as antiparasitic agents since in parasitic protozoa, such as *Trypanosoma cruzi* and *Leishmania* spp., ergosterol is required for cell growth.

Our interest in developing novel approaches to treat diseases caused by parasitic protozoa recently led to the discovery that bisphosphonates of the type used to treat bone resorption diseases are in vitro inhibitors of the growth of *T. cruzi*, *Trypanosoma brucei rhodesiense*, *Leishmania donovani*, *Toxoplasma gondii*, *Plasmodium falciparum*, and *Cryptosporidium parvum*, the causative agents of Chagas' disease, human East African trypanosomiasis, visceral leishmaniasis, toxoplasmosis, malaria, and cryptosporidiosis.[10,11] We also found that the bisphosphonate, risedronate, effects an in vivo cure of *L. donovani* infection in a BALB/c mouse model[12] and that pamidronate effects a parasitological cure of cutaneous leishmaniasis, again in a BALB/c mouse model.[13] These bisphosphonates are, however, only poorly absorbed orally (a few percent). Oral administration is clearly a desirable feature of any drug for use in less-developed nations, and indeed even in developed areas, drugs that are more orally available would be very desirable for treating bone resorption diseases.

* To whom correspondence should be addressed. Tel.: (217)333-3374. Fax: (217)244-0997. E-mail: eo@chad.scs.uiuc.edu.
[†] University of Illinois at Urbana−Champaign.
[‡] Tohoku University.

10.1021/jm010412y CCC: $22.00
Published on Web 04/20/2002

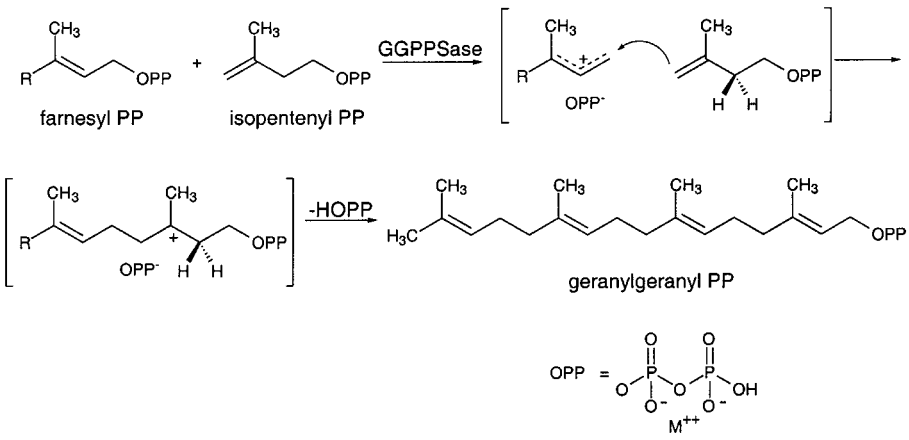

Figure 1. Isoprene chain extension reaction catalyzed by geranylgeranyl PP synthase: Ionization of farnesyl PP generates the first of two carbocation intermediates. Condensation with isopentenyl PP gives rise to a second carbocation that undergoes proton elimination to form geranylgeranyl PP. FPP can also be produced by the enzyme from GPP and IPP.

Because protein geranylgeranylation is of key importance in bone resorption,[14] we reasoned that a more direct approach to developing new chemotherapeutic agents would be to investigate GGPPSase inhibitors. In this context, it was reported some time ago that native GGPPSases from rat liver and in rat brain homogenates are inhibited by the aza-carbocation analogue 3-aza-2,3-dihydrogeranylgeranyl diphosphate (3-azaGGPP, **5**).[15] This inhibitor has a considerably longer carbon chain than the conventional nitrogen-containing bisphosphonates currently in use in bone resorption therapy, which also have substantial activity against a broad spectrum of parasitic protozoa, so the activity of this compound suggested that GGPPSase might represent a useful new target. In addition, the more lipophilic nature of typical GGPPSase inhibitors such as 3-azaGGPP (**5**) might have the added advantage of improved absorption relative to nitrogen-containing bisphosphonates in current use.

The Tohoku group recently reported the cloning, expression, and partial characterization of a human GGPPSase, which catalyzes the condensation of geranyl diphosphate (GPP) or FPP with isopentenyl diphosphate (IPP) to give the C_{20} polyprenyl PP homologue.[16] Although FPPSase and GGPPSase have only a 16% sequence identity, the five conserved amino acid motifs characteristic of trans-prenyl transferases are present in both proteins. Consequently, it appears reasonable to suppose that the mechanisms of the reactions they catalyze are similar and proceed through analogous carbocation$^+$/OPP$^-$ ion pairs, as illustrated in Figure 1.[17] Therefore, it seemed likely that bisphosphonates and related compounds that mimic these or related carbocation intermediates might have similar inhibitory effects on GGPPSase.

In this article, we report the first results on the inhibition of a human recombinant GGPPSase by bisphosphonates and azaprenyl diphosphates. The IC_{50} values range from 140 nM to ~690 μM. We also report the results of a three-dimensional quantitative structure−activity relationship (3D-QSAR)/comparative molecular field analysis (CoMFA) of the inhibitory activity of these compounds, together with predictions of the inhibitory activities of three sets of three compound test sets against GGPPSase using 3D-QSAR/CoMFA and Catalyst[18] pharmacophore modeling approaches.

Synthetic Methods

Procedures developed previously for a six step synthesis of 3-azaGGPP (**5**) from farnesol[15] were adapted to the preparation of the shorter chain polyene amino diphosphates, 3-azaFPP (**6**) and 3-azaGPP (**7**), as shown in eq 1. The principal difference was the use of *N*-methyl-*N*′-*tert*-butylformamidine in place of the corresponding *N*′-cyclohexyl derivative in the nucleophilic aminomethylation step by Meyers' lithioformamidine method.[19] This change was made to facilitate separation of the relatively volatile amine **2c** from the primary amine byproduct generated concurrently in the alkaline hydrolysis of the formamidine intermediate. *N*-Alkylation of secondary amines **2b**,**c** with *tert*-butyl bromoacetate (THF, Et_3N), $LiAlH_4$ reductions (ether, 25 °C), conversion to the methanesulfonates (MsCl, CH_2Cl_2, Et_3N, −15 °C), and displacements with tetrabutylammonium pyrophosphate (2.5 equiv, CH_3CN, 25 °C) were conducted according to the published procedures.[15,20]

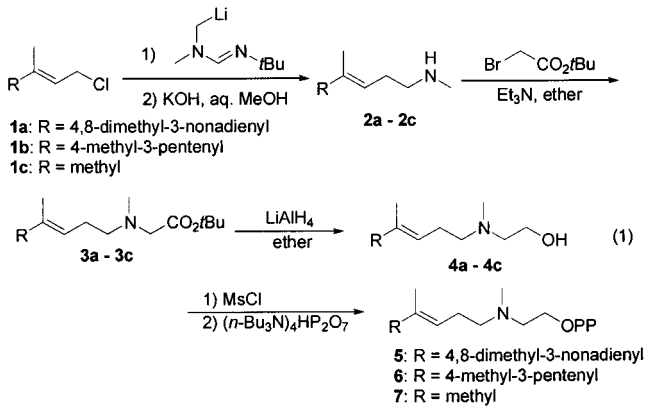

After ion exchange, the hygroscopic ammonium salts, **6** and **7**, were freed from contaminating diphosphate by selective precipitations of the inorganic salt in ammonium bicarbonate buffer. The purities with respect to contamination by inorganic diphosphate and monophosphate as well as other phosphorus-containing impurities were estimated by integration of ^{31}P nuclear magnetic resonance (NMR) spectra. The homologous azaprenyl diphosphates, 3-azahomoGGPP (**11**) and 3-azahomoFPP (**12**), were prepared in similar fashion from amines **2a**,**b** by *N*-alkylation with *tert*-butyl acrylate to

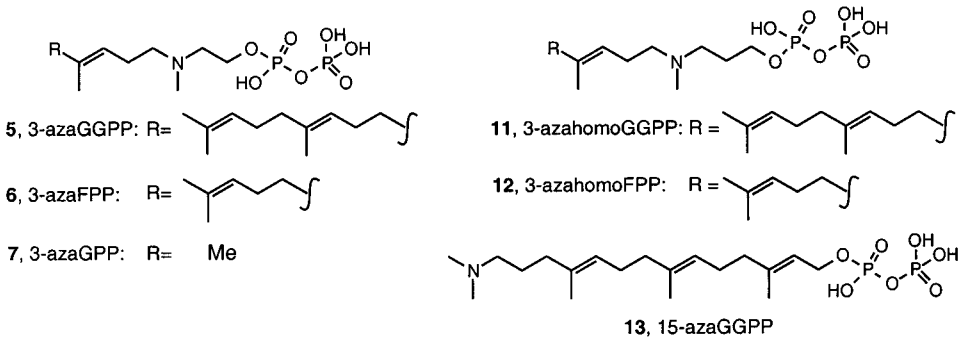

Figure 2. Structures of the six azaprenyl diphosphates investigated.

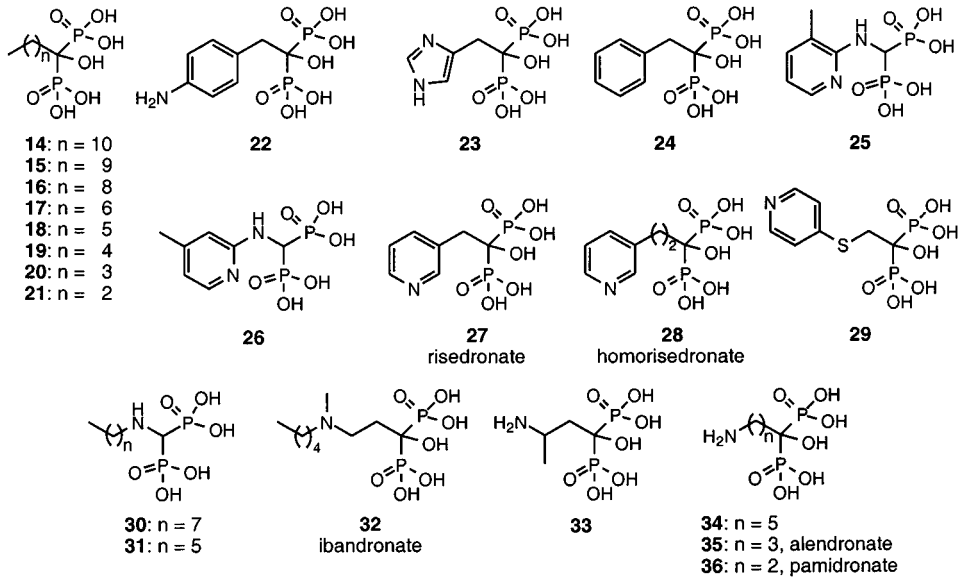

Figure 3. Structures of the 23 bisphosphonates investigated.

the corresponding β-amino propionates **8** and **9** (MeOH, reflux; 70−72%), hydride reductions to tertiary amino alcohols **10a**,**b** (82−91%), and conversion to the diphosphate monoesters by S_N2 displacements of the derived mesylates and/or chlorides (80−81%) (eq 2).

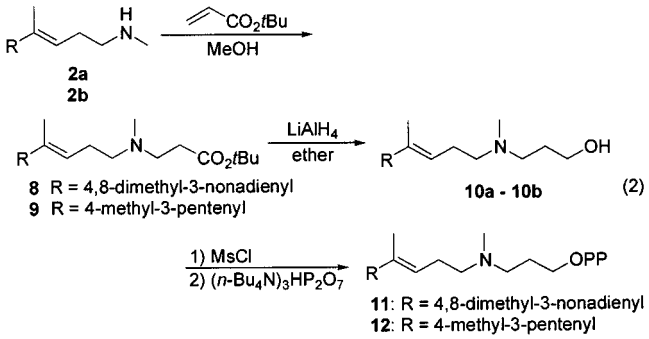

Most of the 1-hydroxymethane-1,1-bisphosphonates shown in Figure 3 were prepared previously by condensation of the corresponding carboxylic acids with phosphorous acid and PCl_3.[10,21] Ibandronate (**32**) was obtained for the present study by phosphonylation of *N*-methyl-*N*-pentyl-3-aminopropionic acid according to this method. The aminomethanebisphosphonates were synthesized from the corresponding primary amines by condensation with ethyl orthoformate and diethyl phosphite followed by acid hydrolysis.[10,22]

Results and Discussion

We investigated the activities of the 29 compounds shown in Figures 2 and 3 in inhibiting the formation of [^{14}C]GGPP from either GPP or FPP, using [^{14}C]IPP substrate. To confirm the formation of radioactive products, one-dimensional thin-layer chromatography (TLC), with autoradiographic detection of [^{14}C]FPP/[^{14}C]GGPP, was used and representative results are shown in Figure 4. The inhibitor concentrations required for 50% enzyme inhibition (the IC_{50} values) were obtained from a graphical fit of the data using a rectangular hyperbolic function. Representative results are shown in Figure 5. The IC_{50} values so obtained are compiled in Table 1 together with the trivial names of several compounds and the code numbers used by the Procter and Gamble Company in their publications.[23] The compound numbers in the text refer to Figures 2 and 3.

The range of activity of these compounds is quite large, 140 nM to ~690 μM, with the most active compounds having similar IC_{50} values to FPPSase inhibitors such as pamidronate and alendronate.[24,25] However, the N-containing bisphosphonates have almost no activity against GGPPSase, Table 2. It is thus of interest to develop more QSARs for GGPPSase (and FPPSase) inhibition to help clarify the origin of these rather large differences (e.g., risedronate, **27**: IC_{50} ~10 nM, FPPSase; ~350 μM, GGPPSase) and potentially to develop more effective drugs.

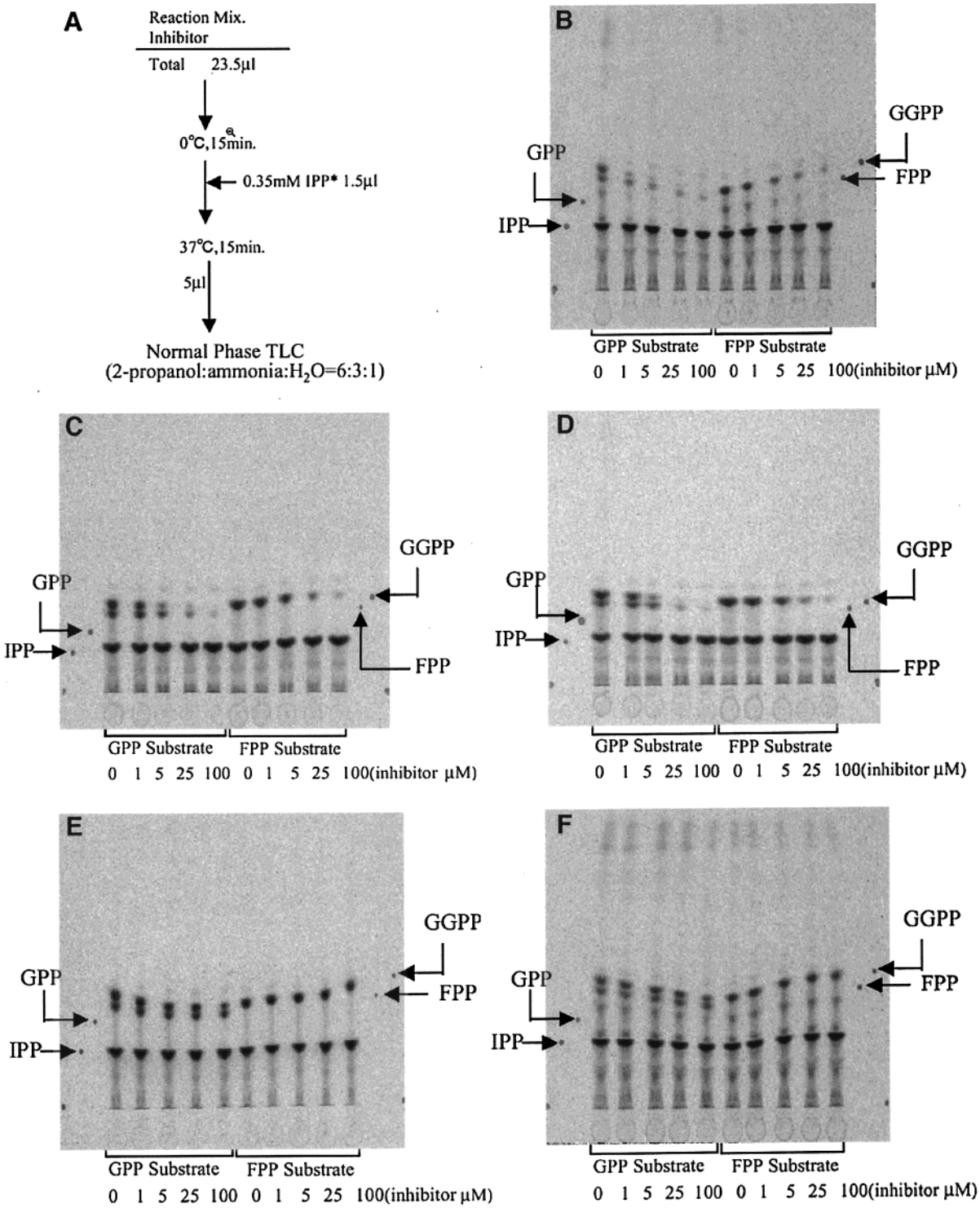

Figure 4. (A) Schematic flowchart for assay of GGPPSase inhibition. (B−F) TLC results for compounds **5**, **30**, **15**, **19**, and **32**, respectively, for [^{14}C]IPP incorporation into FPP and GGPP with GPP substrate (left half of TLC lanes) and [^{14}C]IPP incorporation into GGPP with FPP substrate (right half of TLC lanes). Inhibitor levels used are as indicated.

To begin this process, we first carried out a 3D-QSAR/CoMFA investigation of SARs for the 23 bisphosphonates together with the 5 azaprenyl diphosphates that had measurable activities (Table 1, Figures 2 and 3) to try to deduce which structural factors are most important in GGPPSase inhibition. Each of the bisphosphonate compounds was aligned to the most active bisphosphonate (**16**) acting as a template by performing an rms fitting of the pharmacophoric atoms of each conformer to those of the template by using the shape reference alignment function of the QSAR module of Cerius^2 4.6.[26] The alignments of each of the molecular mechanics geometry-optimized structures, obtained through pairwise superpositioning using the maximum common subgroup (MCSG) method, placed all 23 bisphosphonates in the same reference frame as the shape reference. We used the geometry of GPP bound to the active site of FPPSase[27] as a model with which to build the energy-minimized structure of 3-azaGGPP (**5**). The structures of 3-azaFPP (**6**), 3-azaGPP (**7**), 3-azahomoG-

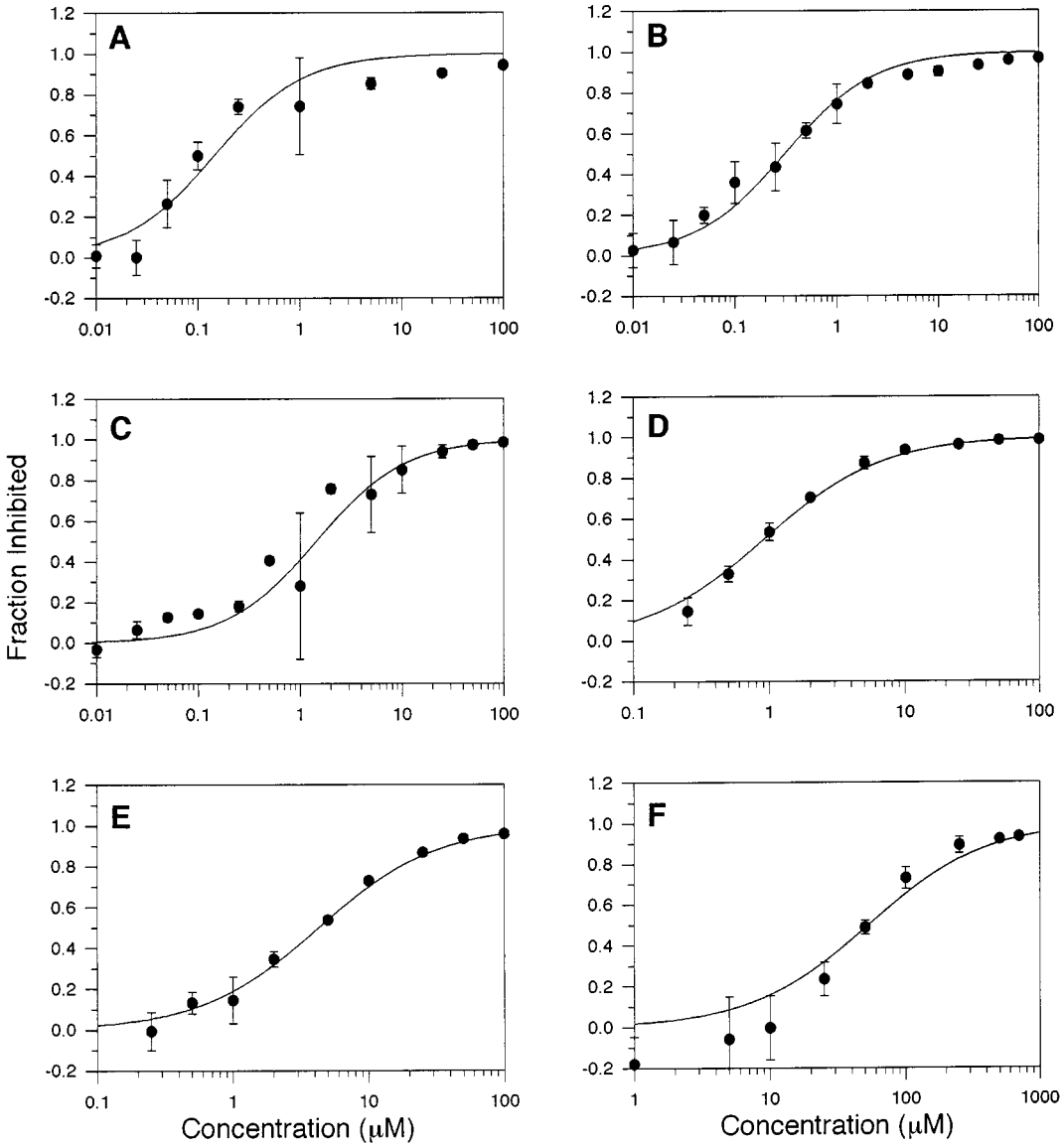

Figure 5. GGPPSase enzyme inhibition by (A) **5**; (B) **12**; (C) **15**; (D) **14**; (E) **17**; and (F) **19** together with least-squares fits to the equation $I = (I_{max}C)/(IC_{50} + C)$ where I is the inhibition fraction, $I_{max} = 1$, C is the concentration of the inhibitor (μM), and IC_{50} is the concentration for 50% inhibition (μM).

GPP (**11**), and 3-azahomoFPP (**12**) were all then built by suitable modifications of **5**. All of the azaprenyl compounds were aligned to the bisphosphonates by performing a least-squares fit in Cerius[2] between four atom centers. Specifically, the two phosphorus atoms, the oxygen adjacent to the prenyl side chain, and C-1 in the azaprenyl diphosphates were aligned to the corresponding phosphorus atoms, C-2, and C-3 in compound **16**. All ring nitrogens in the aromatic species were assumed to be protonated, as were the amino-alkyl side chains in the nonaromatic bisphosphonates (such as ibandronate, **32**), while the phosphonate groups each had a −1 charge. The diphosphate charges were taken to be −2. In the case of the protonated form of **32**, the molecule is chiral: the enantiomer that best fit the overall alignment, (*S*)-ibandronate, was selected for incorporation into the QSAR model. The *S* stereroisomers of the protonated forms of **5**−**7** and **33** and the *R* stereoisomers of the protonated forms of **11** and **12** were also used. The results of the alignment are shown in Figure 6, which includes the superimposition of all training set molecules in order to illustrate the overall alignment of the conformers used. Charges were calculated by using the Gasteiger−Marsili method.[28] We then used 3D-QSAR/CoMFA methodologies, as embodied in the Cerius[2] 4.6 suite of programs, to analyze the inhibition data shown in Table 1. We performed a regression analysis of the inhibition results using the relationship $pIC_{50} = -\log (IC_{50}, M)$ and the genetic function approximation (GFA) algorithm[29] to obtain the following QSAR equation

$$pIC_{50} = 3.55 + 0.44 \times \text{“}CH_3/473\text{”} - 0.37 \times \text{“}CH_3/330\text{”} + 0.04 \times \text{“}CH_3/461\text{”} - 0.01 \times \text{“}H^+/318\text{”} \quad (3)$$

The descriptors H^+, HO^-, and CH_3 represent the corresponding probe interaction energies (electrostatic, hydrogen bond donor/acceptor, and steric, respectively) at defined grid points. The locations of the four grid points appearing in this particular CoMFA equation are shown in Figure 6. As expected, there are no points

Table 1. Experimental IC_{50}, pIC_{50}, and Predicted pIC_{50} Values for GGPPSase Inhibitors and Statistical Results of 3D-QSAR CoMFA and Catalyst Models (See Figures 2 and 3 for Compound Structures)

			3D-QSAR/CoMFA predicted pIC_{50}[a]				Catalyst predicted pIC_{50}[a]			
	experimental activity		28 compd				28 compd training set			
compd	IC_{50} (μM)	pIC_{50}	training set	3 compd test sets			3 compd test sets			
5 (3-azaGGPP)	0.14 ± 0.03	6.84	6.50	6.55	6.46	6.55	6.25	6.32	6.59	6.54
12 (3-azahomoFPP)	0.31 ± 0.02	6.51	6.15	6.20	**6.08**	6.50	6.46	6.48	**6.51**	6.54
11 (3-azahomoGGPP)	0.37 ± 0.03	6.43	6.32	6.37	6.26	6.09	6.43	6.46	6.57	6.68
16	0.72 ± 0.02	6.14	6.15	6.20	6.08	6.09	5.85	6.25	5.74	5.85
6 (3-azaFPP)	0.74 ± 0.04	6.13	6.51	6.55	6.46	6.56	6.22	6.30	6.55	6.54
14	0.92 ± 0.03	6.04	6.15	6.20	6.08	**6.09**	6.03	6.27	5.89	**5.89**
15	1.4 ± 0.2	5.84	6.15	**6.20**	6.08	6.09	6.01	**6.25**	5.74	5.85
30	2.2 ± 0.2	5.66	5.87	5.91	5.75	5.84	5.92	6.23	5.64	5.85
17	4.3 ± 0.4	5.37	5.06	5.10	**4.97**	4.99	4.85	4.80	**4.77**	4.85
18	11 ± 1	4.95	4.17	4.17	4.18	4.07	4.85	4.80	4.77	**4.80**
31	19 ± 1	4.72	4.86	**4.91**	4.76	4.79	5.00	**4.89**	4.89	4.96
19	53 ± 6	4.28	3.91	3.90	3.95	3.80	3.82	4.08	4.00	3.82
32 (ibandronate)	83 ± 13	4.08	3.72	3.72	3.74	3.68	4.48	4.42	4.27	4.47
36 (pamidronate)	180 ± 20	3.75	3.65	3.64	3.67	3.57	3.44	3.43	3.41	3.42
22	180 ± 60	3.73	3.33	3.33	3.33	3.50	3.43	3.44	3.41	3.43
20	200 ± 40	3.70	3.91	3.90	3.96	3.81	3.43	3.43	3.41	3.42
24	220 ± 50	3.66	3.92	3.90	**3.96**	3.81	3.43	3.43	**3.41**	3.42
23	220 ± 40	3.66	3.60	3.60	3.62	3.57	3.44	3.44	3.41	3.43
25	220 ± 50	3.66	3.61	3.61	3.63	3.56	3.44	3.43	3.41	3.42
7 (3-azaGPP)	240 ± 20	3.62	3.73	3.78	3.64	3.73	4.89	4.96	4.89	4.89
26	260 ± 20	3.58	3.62	3.61	3.64	3.56	3.85	4.20	4.11	3.92
33	330 ± 90	3.49	3.63	3.63	3.65	3.57	3.43	3.43	3.41	3.42
27 (NE58095, risedronate)	350 ± 50	3.45	3.47	3.47	3.48	**3.52**	3.43	3.43	3.41	**3.42**
28 (NE58051, homorisedronate)	410 ± 130	3.39	3.33	**3.33**	3.32	3.39	3.43	**3.43**	3.41	3.42
35 (alendronate)	440 ± 60	3.36	3.54	3.54	3.55	3.50	3.44	3.44	3.41	3.43
29	550 ± 200	3.26	3.58	3.57	3.59	3.45	3.44	3.43	3.41	3.42
21	620 ± 270	3.21	3.92	3.90	3.96	3.81	3.43	3.43	3.41	3.42
34	690 ± 370	3.16	3.32	3.33	3.29	3.40	3.43	3.43	3.41	3.42
13 (15-azaGGPP)	≫ 100									
R^2[b]			0.938	0.936	0.938	0.956	0.914	0.899	0.913	0.911
F_{test}[c]			86.8	73.7	75.1	108.7				
R_{cv}^2[d]			0.900	0.845	0.907	0.921				
R_{bs}^2[e]			0.938	0.937	0.938	0.956				
N[f]			5	5	5	5				
N[g]			28	25	25	25	28	25	25	25

[a] Bold values represent predicted activities of compounds that were not included in the training set. [b] Correlation coefficient. [c] Ratio of R^2 explained to unexplained = $R^2/(1 - R^2)$. [d] Cross-validated correlation coefficient after leave-one-out procedure. [e] Average squared correlation coefficient calculated during the validation procedure. [f] Optimal number of principal components. [g] Number of compounds.

Table 2. Comparison of Bisphosphonate Inhibitory Activities against Human Recombinant FPPSase and GGPPSase (See Figure 3 for Compound Structures)

	experimental activity, IC_{50} (μM)	
compd	FPPSase[a]	GGPPSase[b]
32 (ibandronate)	0.02	83 ± 13
36 (pamidronate)	0.20	180 ± 20
27 (risedronate)	0.01	350 ± 50
28 (homorisedronate)	2.93	410 ± 130
35 (alendronate)	0.05	440 ± 55

[a] From ref 24. [b] From Table 1.

associated with the bisphosphonate/diphosphate headgroup, since these highly polar motifs are common to all of the compounds studied and consequently do not contribute significantly to the range of activity seen in GGPPSase inhibition. As shown in Table 1 and Figure 7A, the GFA method provided a good QSAR correlation between experimental and predicted pIC_{50} values with an R^2 of 0.938 and a cross-validation R_{cv}^2 of 0.900. The optimal number of components in the final GFA model (=5) was determined using cross-validated R^2 and standard error prediction analyses, as obtained from the leave-one-out cross-validation technique.[30] We decided to proceed further and investigate the actual predictive utility of the QSAR model, which if successful should facilitate the design of additional GGPPSase inhibitors.

To test the predictive ability, we removed three compounds from the training set prior to GFA analysis. The resulting model based on the reduced training set was then used to predict the activities of the three excluded compounds. This procedure was repeated three times using different test sets, and the predicted IC_{50} values are shown in bold in Table 1. The three compounds in each test set were chosen at random while maintaining a distribution of activities. In Figure 7B, we show graphical results for the three training sets (○) together with the three test set points (■). The QSAR equations for the three training sets were

$$pIC_{50} = 3.54 + 0.44 \times \text{“}CH_3/473\text{”} - 0.38 \times \text{“}CH_3/330\text{”} + 0.04 \times \text{“}CH_3/461\text{”} - 0.01 \times \text{“}H^+/318\text{”} \quad (4)$$

$$pIC_{50} = 3.56 + 0.43 \times \text{“}CH_3/473\text{”} - 0.36 \times \text{“}CH_3/330\text{”} + 0.03 \times \text{“}CH_3/461\text{”} - 0.01 \times \text{“}H^+/318\text{”} \quad (5)$$

$$pIC_{50} = 3.46 + 0.45 \times \text{“}CH_3/473\text{”} - 0.39 \times \text{“}CH_3/330\text{”} + 0.04 \times \text{“}CH_3/461\text{”} - 0.01 \times \text{“}H^+/344\text{”} \quad (6)$$

Statistical data for all QSAR equations are given in

Table 1. The rms error in predicted pIC_{50} of the test set compounds was 0.39, which corresponds to a factor of ~2.5 in predicting the experimental IC_{50} values over the ~700 μM range in activity tested in Table 1. Using solely the nine predicted test set points, the correlation between experiment and prediction is $R^2 = 0.882$.

SARs. The library of compounds investigated contains many diverse structural features: ionic bisphosphonate and diphosphate groups; alkyl, alkenyl (prenyl), aryl, and heteroaryl side chains; 1-OH- and 1-H-bearing bisphosphonates; and nitrogen-containing or nitrogen-free side chains, together with different locations of the side chain nitrogens. With so many diverse structural features, QSAR methods are clearly desirable in order to begin to predict in a quantitative manner inhibitory activity over a wide range of values, but of course, it is also helpful to draw at least some more qualitative structural conclusions from an inspection of all of the results, to guide future inhibitor design. Here, we briefly outline some of the trends that are apparent.

First, it is evident that all eight aromatic bisphosphonates are extremely poor inhibitors of GGPPSase, even though several of them have low nanomolar IC_{50} values vs FPPSase. Second, the short alkyl chain nitrogen-containing bisphosphonates are also poor inhibitors. As shown in Table 1, ibandronate (**32**) has an 83 μM IC_{50} vs GGPPSase but only a 20 nM IC_{50} vs FPPSase.[24] These results might imply a rather different local structure in the GGPPSase and FPPSase E·I complexes or even different modes of binding. Alternatively, perhaps the side chains in the known potent FPPSase inhibitors are simply too short to act as competitive inhibitors since the substrate (FPP) has a 15 carbon side chain (or at least a continuous 12 carbon fragment) that can be expected to play an important role in binding to the active site, due to van der Waals dispersion forces or hydrophobic bonding. In the GGPPSase 3D-QSAR CoMFA, CH_3—probe (van der Waals) interactions are clearly of importance, as may be seen in eq 3—6 above, while in FPPSase 3D-QSAR CoMFA models,[31] electrostatic interactions appear to be more important. Third, our results clearly confirm the importance of hydrophobic interactions in the case of the *n*-alkyl 1-hydroxy-1,1-bisphosphonates. As the *n*-alkyl chain length increases, the IC_{50} values decrease essentially monotonically, from ~620 μM for C_3 to ~1 μM for C_9, C_{10}, and C_{11}. Fourth, the strong inhibition by 3-azaGGPP (IC_{50} = 140 nM) is similar to that previously reported for the effect of this amino diphosphate on native GGPPSase from rat liver (90% inhibition at 0.9 μM).[15a] This potency is perhaps not surprising in view of its close resemblance to GGPP and the previous observation of product inhibition with bovine brain GGPPSase (K_i = 1.2 μM).[32]

The various isoprenoid amino diphosphates **5**, **6**, **11**, and **12** might interact with the GGPPSase active site in one of several ways: as analogues of the FPP substrate (S_1), as analogues of either of the two different carbocation diphosphate ion pair intermediates, or as analogues of the GGPP product. If the mechanism follows the ionization—condensation—elimination sequence proposed by Poulter and co-workers for FPPSase,[17,33] the prenyl extension reaction would be initiated by formation of a farnesyl$^+$/OPP$^-$ ion pair, and the second carbocation would be formed in the following condensation step with IPP (Figure 1). The sequence of reactions is clearly complex, but we have synthesized several homologues of azaprenyl FPP and GGPP, which allow us to test the hypothesis that these compounds are acting as carbocation intermediate analogues. First, the additional methylene group in 3-azahomoFPP (**12**) would increase the charge separation between ammonium and diphosphate moieties so that the product would more closely resemble the putative farnesyl$^+$/OPP$^-$ ion pair intermediate, as illustrated in Figure 8A. The experimental values of 740 nM for **6** but 310 nM for **12** are consistent with this idea. Second, in the case of the GGPP analogues (Figure 8B), we anticipated that 3-azaGGPP (**5**) might mimic the geranylgeranyl pyrophosphate carbocation (E·I) prior to release from the enzyme, while 3-azahomoGGPP (**11**) would be a worse inhibitor, since it would mimic a C_{25} synthase inhibitor. The experimental results support this idea since the IC_{50} values for 3-azaGGPP (**5**) and 3-azahomoGGPP (**11**) are 140 and 370 nM, respectively. These trends are not seen in our QSAR modeling; however, this is most likely because the CoMFA (or Catalyst) IC_{50} predictions have about a factor of 2—2.5 error (see below). The chain terminus analogue 15-aza GGPP (**13**) showed no inhibition at 100 μM, which evidently reflects the incompatibility of its charged terminus with the interior of the hydrophobic polyene binding pocket.

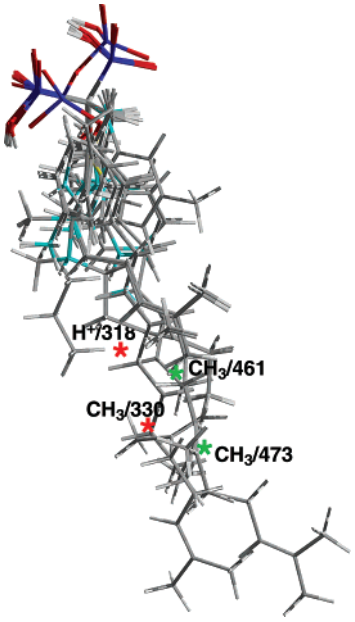

Figure 6. MCSG alignment of the 28 molecules that had quantitatively measurable activities together with the locations of the four descriptors given in eq 3. The alignments used **16** as the shape reference compound, as discussed in detail in the text.

Catalyst Pharmacophore Investigations. The results presented above indicate that 3D-QSAR/CoMFA methodologies permit relatively accurate predictions of the activity of the bisphosphonate and diphosphate GGPPSase inhibitors investigated. However, we only investigated the single alignment described above, and clearly, other alignments are possible. A convenient approach to investigating multiple alignments is to use the Catalyst[18,34] approach in which large numbers of inhibitor conformations are considered and numerous

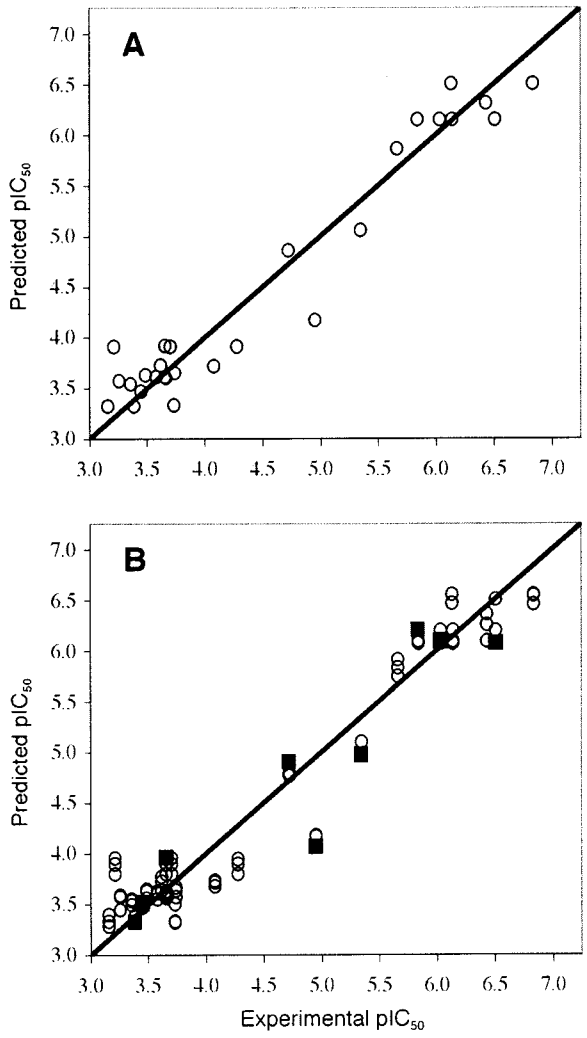

Figure 7. Graphical comparisons between experimental and predicted pIC_{50} values for GGPPSase inhibition. (A) A 28 compound training set. (B) Superposition of three sets of predictions for test set (■) and training set (○) compounds. For the test set only, $R^2 = 0.882$ and rms error = 0.39.

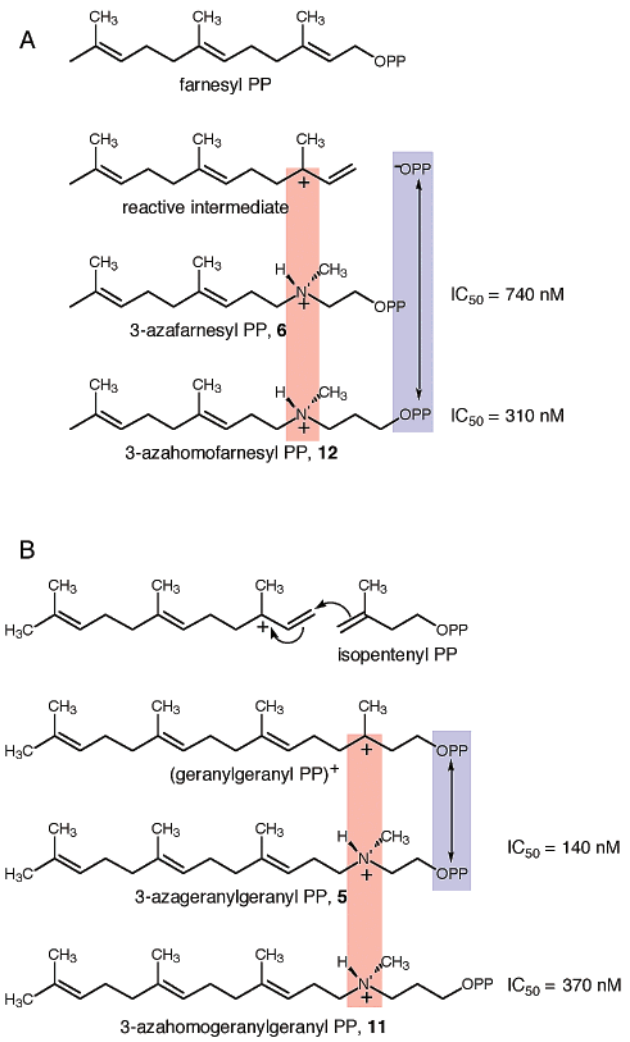

Figure 8. Schematic showing a comparison between (A) 3-azaFPP (**6**) and 3-azahomoFPP (**12**) structures with FPP and the putative carbocation−pyrophosphate ion pair. (B) 3-azaGGPP (**5**) and 3-azahomoGGPP (**11**) with the putative $(GGPPH)^+$ carbocation formed from FPP^+ and IPP. The 3azaGGPP species is thought to mimic the $(GGPPH)^+$ carbocation.

pharmacophore hypotheses are generated. This approach has not only predictive utility but also provides a potentially useful graphical representation of the key structural features of a pharmacophore, suitable for virtual screening.

We therefore generated a pharmacophoric model for all compounds using the Hypogen module in the Catalyst software package.[18] To facilitate feature recognition, we used the structures from the 3D-QSAR/CoMFA model with explicitly defined single and double P−O bonds. Activity uncertainities of 3.0 (Catalyst default) were used for all compounds. Hydrophobic, negative ionizable, and positive charge features were considered for hypothesis generation, since these features are common among the most active compounds. We required hypotheses to have two negative ionizable groups in order to account for the bidentate interactions of diphosphates observed in the crystal structures of FPPS.[27] While numerous hypotheses were generated, they all typically had quite similar features, with two negative ionizable groups and two or three hydrophobic features. One representative hypothesis is illustrated in Figure 9 in which the light blue spheres represent the two hydrophobic features while the dark blue spheres represent the two negative ionizable groups. This hypothesis is shown superimposed on (A) 3-azaGGPP (**5**), (B) **17**, and (C) risedronate (**27**) in Figure 9. This figure clearly illustrates the key importance of the hydrophobic interactions in controlling activity. Compounds **5** and **17** have two and one hydrophobic "matches", respectively, while risedronate (**27**) has none. This agrees with the increasing IC_{50} values of 140 nM, 4.3, and 350 μM, respectively, and similar low activities are predicted for other potent FPPSase inhibitors; see Table 2.

To further judge the predictive ability of this pharmacophore model, we again used the three training sets described above (results given in Table 1) to generate hypotheses containing two negative ionizable and two hydrophobic features to predict the activities of three sets of three test compounds, this time employing the Catalyst program. We found an R^2 value of 0.948 between experiment and prediction (see Figure 10), together with a 0.28 pIC_{50} rms error. We did not investigate numerous other alignments, conformations, or hypotheses in either the Catalyst or the CoMFA

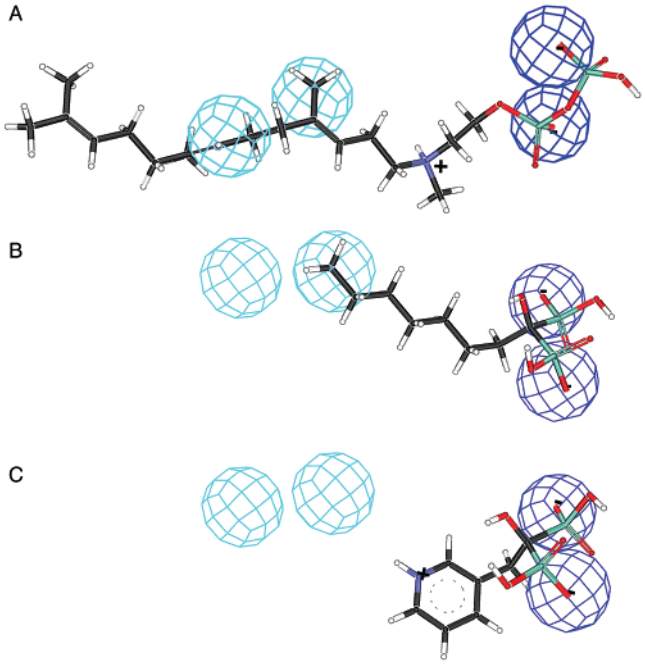

Figure 9. Catalyst pharmacophore hypothesis for GGPPSase inhibition by bisphosphonates and diphosphates. The light blue spheres represent hydrophobic components of the hypothesis, and the dark blue spheres represent negative ionizable components. Pharmacophore superimposed on (A) 3-azaGGPP (**5**); (B) **17**; and (C) risedronate (**27**).

methods, since the results already appeared quite respectable.

When taken together, these results clearly indicate that long chain alkyl bisphosphonates and related compounds can act as inhibitors of GGPPSase. While the IC_{50} values of most of the compounds investigated in this initial study are higher than those of the most potent FPPSase inhibitors, the IC_{50} values for the isoprenoid amino diphosphates are equal to or lower than those of pamidronate and alendronate ($IC_{50} \approx 0.2-0.5\ \mu M$), drugs widely used in bone resorption therapy. Because the longer chain inhibitors we have investigated are quite lipophilic, they can be expected to have improved absorption characteristics and may thus represent a novel approach to the design of bone antiresorption and antiparasitic agents.

Conclusions

The results described above are of interest for a number of reasons. First, we have carried out a detailed study of the inhibition of an enzyme in the isoprenoid biosynthetic pathway, GGPPSase, by a broad range of bisphosphonate inhibitors and azaprenyl diphosphate analogues. The range of IC_{50} values varies from 140 nM to ~690 μM. Second, we have carried out the first QSAR study of the inhibition of GGPP synthase using 3D-QSAR/CoMFA techniques. The results show good agreement between experimental and predicted pIC_{50} values ($R^2 = 0.938$, $R_{cv}^2 = 0.900$, $R_{bs}^2 = 0.938$, and F-test = 86.8), and the method has predictive utility as evidenced by prediction of the activity of nine test set compounds with an rms pIC_{50} error of 0.39. Third, an analysis of the CoMFA inhibition results clearly indicates the importance of van der Waals interactions in GGPPSase inhibition. Fourth, using Catalyst, we developed a

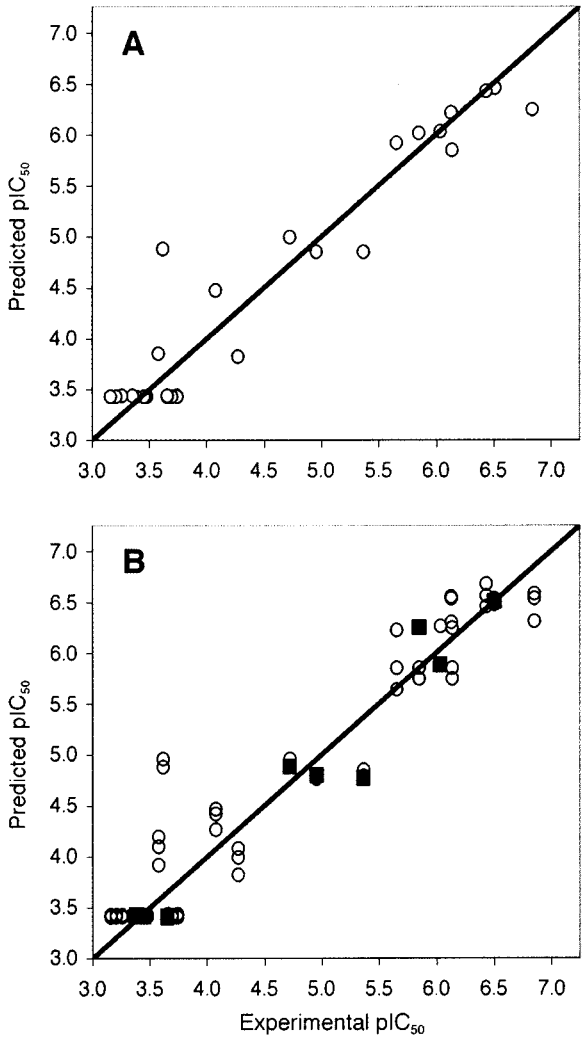

Figure 10. Graph showing correlation between experimental and Catalyst predicted pIC_{50} values. (A) A 28 compound training set. (B) Superposition of three sets of predictions for test set (■) and training set (○) compounds. For the test set only, $R^2 = 0.948$ and rms error = 0.28.

pharmacophore model (hypothesis) for GGPPSase inhibition that also had promising predictive ability and confirmed the importance of hydrophobic interactions in GGPPSase inhibition together with, as expected, the importance of negative ionizable groups. Overall, given the important role of geranylgeranylation in osteoclast function (bone resorption) as well as in the growth of parasitic protozoa, these results imply that GGPPSase inhibitors appear to be attractive candidates for the development of future drugs, which can be expected to have improved absorption characteristics due to their more lipophilic character.

Experimental Section

Inhibitors. Experimental procedures and characterization data are provided below for 3-azaFPP (**6**) (eq 1) and 3-azahomoFPP (**12**) (eq 2). Purities of the 3-azaprenyl and 3-azahomoprenyl PPs were judged to be ≥90−95% from inspection and integration of their ^1H and ^{31}P NMR spectra (see Supporting Information). 15-azaGGPP (**13**) was available from previous work.[35]

Samples of bisphosphonates **14**−**29**, **31**, and **33**−**36** were available from previous work.[10] The purity of all bisphosphonates was verified by microchemical analysis (H/C/N/P) and via ^{13}C, ^{31}P, and ^1H NMR spectroscopy; the ^1H NMR experi-

ments were performed in triplicate using an internal maleic acid quantitation standard.

***N*-Methyl-4,8-dimethyl-3*E*,7*E*-nonadien-1-amine (2b).** The procedure was based on the literature.[15b,36] Lithiation of *N*′-*tert*-butyl-*N*,*N*-dimethylformamidine (2.4 g, 18.8 mmol) in dry THF (60 mL) with *tert*-butyllithium (13 mL, 1.7 M, 22.1 mmol) in pentane at −25 °C for 1 h was followed by alkylation with geranyl chloride (2.9 g, 17 mmol) in THF (10 mL) at −78 °C to room temperature (2 h). Hydrolysis of the crude formamidine in 4:1 methanol−water (70 mL) containing KOH (4.8 g, 85 mmol) at reflux (ca. 12 h) afforded amine **2b** (2.7 g, 95%) as a colorless oil, which was used without further purification. TLC R_f 0.12 (33% MeOH/CH_2Cl_2). ^{1}H NMR, ^{13}C NMR, and IR data agreed with the literature values.[15b]

1,1-Dimethylethyl 2-[*N*-Methyl-*N*-[4,8-dimethyl-3*E*,7*E*-nonadienyl]amino]ethanoate (3b). Alkylation of amine (2.7 g, 16.2 mmol) with *tert*-butyl bromoacetate (3.3 g, 17.0 mmol) in the presence of triethylamine (1.8 g, 17.8 mmol) in dry THF (18 mL) under N_2 was carried out by a literature procedure.[15b] Purification of the crude product by column chromatography with 50% ether/pentane gave 4.1 g (90%) of the known amino ester **3b** as a colorless oil. TLC R_f 0.63 (33% EA/hexane). ^{1}H NMR, ^{13}C NMR, and IR data agreed with the literature values.[15b]

2-[*N*-Methyl-*N*-[4,8-dimethyl-3*E*,7*E*-nonadienyl]amino]-ethanol (4b). The procedure was based on the literature for a related compound.[15b] A suspension of $LiAlH_4$ (742 mg, 19.5 mmol) in dry ether (50 mL) under N_2 was stirred and cooled at 0 °C as amino ester **3b** (1.7 g, 5.9 mmol) in ether (15 mL) was added dropwise. The mixture was stirred at room temperature for 2 h and cooled to 0 °C. Water (0.8 mL), 15% aqueous KOH (0.8 mL), and water (2.2 mL) were added in succession.[37] After it was stirred at room temperature for 1 h, the insoluble salts were removed by filtration, and the filtrate was concentrated. Purification by column chromatography with 50% ether/pentane gave 1.3 g (94%) of amino alcohol **4b** as a colorless oil. TLC R_f 0.35 (33% MeOH/CH_2Cl_2). ^{1}H NMR (500 MHz, $CDCl_3$): δ 5.08−5.01 (m, 2 H), 3.53 (t, 2 H, J = 5.4), 3.22 (br. s, 1 H), 2.48 (t, 2 H, J = 5.4), 2.37 (t, 2 H, J = 7.1), 2.22 (s, 3 H), 2.12 (q, 2 H, J = 7.5), 2.01 (q, 2 H, J = 7.5), 1.93 (t, 2 H, J = 8.1), 1.62 (s, 3 H), 1.57 (s, 3 H), 1.55 (s, 3 H). ^{13}C NMR (125 MHz, $CDCl_3$): δ 136.3, 131.2, 124.1, 121.6, 58.6, 58.3, 57.4, 41.5, 39.6, 26.5, 25.8, 25.5, 17.5, 15.9. IR (thin film): ν_{max} 3421, 2966, 2923, 2854, 2798, 1668, 1452, 1376, 1041 cm^{-1}. EIMS: m/z 226.2 $[M + H]^+$ (1), 194.2 (2), 124.1 (1), 88.1 (100), 69.1 (9), 57.0 (5). HREIMS: m/z 224.2018 (calcd for $C_{14}H_{26}NO$, $[M - H]^+$ 224.2014).

2-[*N*-Methyl-*N*-[4,8-dimethyl-3*E*,7*E*-nonadienyl]amino]-ethyl Diphosphate (3-azaFPP, 6). Literature methods[20] were used with some modifications including omission of the cellulose column chromatography step. A solution of amino alcohol **4b** (257 mg, 1.1 mmol) and triethylamine (173 mg, 173 mmol) in dry CH_2Cl_2 (11 mL) under N_2 was stirred and cooled at −15 °C as methanesulfonyl chloride (0.1 mL, 1.3 mmol) was added dropwise. After 0.5 h, the product was extracted with ice-cold CH_2Cl_2 (10 mL). The organic layer was washed with ice-cold saturated $NaHCO_3$ (2 × 10 mL), dried ($MgSO_4$), and concentrated to 5 mL. MeCN (15 mL) was added to the solution of mesylate/chloride in CH_2Cl_2 (5 mL). The solution was concentrated to 2 mL and stirred in an ice bath as tris(tetra-*n*-butyl)ammonium hydrogen pyrophosphate (2.7 g, 2.8 mmol) in MeCN (3 mL) was added. The suspension was stirred at room temperature for 6 h. After it was washed with pentane (3 × 10 mL) and concentrated, the residue was dissolved in 2 mL of ion exchange buffer (25 mM NH_4HCO_3 containing 2% (v/v) 2-propanol). The resulting solution was passed through a column (2 cm × 10 cm) of Dowex AG 50W-X8 (100−200 mesh) cation-exchange resin (ammonium form). The column was eluted with 2 column volumes of ion exchange buffer, and the eluant was lyophilized to dryness. The residual white solid was partially dissolved in 20 mL of 3:5:5 (v/v/v) 25 mM aqueous NH_4HCO_3−MeCN−2-propanol. The gellike mixture was vortexed, the suspension was centrifuged, and the supernatant solution was decanted into another round-bottomed flask. The extractions were repeated ≥5 times until a white solid was completely formed. The extraction sequence was then repeated with 4:5:5 (v/v/v) 25 mM aqueous NH_4HCO_3/CH_3CN/2-propanol. The combined supernant solutions were concentrated to near dryness by rotary evaporation. The solid was dissolved in 25 mM NH_4HCO_3 (10 mL), and the solution was lyophilized to dryness to give 3-aza FPP **6** (308 mg, 60% yield, 91% purity by ^{31}P NMR) as a white solid. ^{1}H NMR (500 MHz, ND_4OD/D_2O): δ 5.01 (br, 2 H), 4.18 (br, 2 H), 3.35 (br, 2 H), 3.03 (br, 2 H), 2.83 (s, 3 H), 2.39 (br, 2 H), 1.97 (q, 2 H, J = 6.2), 1.90 (br, 2 H), 1.57 (s, 3 H), 1.55 (s, 3 H), 1.49 (s, 3 H). ^{13}C NMR (125 MHz, ND_4OD/D_2O): δ 139.3, 131.2, 124.2 (d, J = 7.4), 118.0 (d, J = 5.5), 59.5, 55.4 (d, J = 17.5), 39.5 (d, J = 8.3), 39.1, 38.4 (d, J = 9.2), 26.0, 25.1 (d, J = 6.4), 22.1, 17.0 (d, J = 6.4), 15.4 (d, J = 6.4). ^{31}P NMR (202 MHz, ND_4OD/D_2O): δ −6.34 (d, 1 P, J = 19.8), −10.02 (d, 1 P, J = 19.8). LRFABMS (H_2O): m/z 386.2. HRFABMS (positive ion) calcd for $C_{14}H_{30}NO_7P_2$, 386.1498; found, 386.1498. The ^{31}P NMR spectrum showed an extra peak attributed to inorganic pyrophosphate [δ_P −7.49 (s, 0.09 P)].

1,1-Dimethylethyl 3-[*N*-Methyl-*N*-[4,8-dimethyl-3*E*,7*E*-nonadienyl]amino]propanoate (9). The procedure was based on a literature procedure for a different compound.[38] A solution of the *N*-methylamine **2b** (715 mg, 4.3 mmol) in dry MeOH (15 mL) under N_2 was stirred at room temperature as *tert*-butyl acrylate (1.1 mL, 8.5 mmol) was added. The solution was refluxed for 1 day. After it was concentrated under reduced pressure, the residue was subjected to column chromatography with 33% EA/hexane to give 913 mg (72%) of the *β*-amino ester **9** as a colorless oil. TLC R_f 0.40 (33% EA/hexane). ^{1}H NMR (500 MHz, $CDCl_3$): δ 5.09−5.03 (m, 2 H), 2.65 (t, 2 H, J = 7.3), 2.35 (t, 2 H, J = 7.7), 2.32 (t, 2 H, J = 7.5), 2.21 (s, 3 H), 2.12 (q, 2 H, J = 7.9), 2.03 (q, 2 H, J = 7.9), 1.94 (t, 2 H, J = 8.1), 1.64 (d, 3 H, J = 1.1), 1.58 (s, 3 H), 1.56 (s, 3 H), 1.41 (s, 9 H). ^{13}C NMR (125 MHz, $CDCl_3$): δ 172.0, 136.2, 131.3, 124.2, 121.7, 80.2, 57.2, 52.8, 41.8, 39.6, 33.6, 28.0, 26.6, 26.0, 25.6, 17.6, 16.0. IR (thin film): ν_{max} 2975, 2927, 2852, 2795, 1731, 1454, 1367, 1255, 1155, 1039, 848 cm^{-1}. EIMS: m/z 310.5 $[M + H]^+$ (1), 254.2 (1), 236.2 (3), 194.2 (13), 172.1 (40), 116.1 (100), 88.1 (1), 74.1 (9), 57.1 (5). HREIMS: m/z 308.2586 (calcd for $C_{19}H_{34}NO_2$ $[M - H]^+$ 308.2590).

3-[*N*-Methyl-*N*-[4,8-dimethyl-3*E*,7*E*-nonadienyl]amino]-propanol (10b). The $LiAlH_4$ reduction of **9** was carried out as described above for **4b**. Yield, 389 mg (91%). TLC R_f 0.35 (33% MeOH/CH_2Cl_2). ^{1}H NMR (500 MHz, $CDCl_3$): δ 5.09−5.03 (m, 2 H), 3.76 (t, 2 H, J = 5.1), 2.57 (t, 2 H, J = 5.6), 2.35 (t, 2 H, J = 7.3), 2.23 (s, 3 H), 2.15 (q, 2 H, J = 7.7), 2.04 (q, 2 H, J = 7.7), 1.95 (t, 2 H, J = 7.9), 1.66 (quintet, 2 H, J = 5.1), 1.64 (s, 3 H), 1.59 (s, 3 H), 1.57 (s, 9 H). ^{13}C NMR (125 MHz, $CDCl_3$): δ 136.5, 131.2, 124.2, 121.3, 64.6, 58.3, 57.8, 41.8, 39.6, 27.6, 26.5, 25.8, 25.6, 17.6, 15.9. IR (thin film): ν_{max} 3378 (−OH), 2925, 2852, 2800, 1668, 1452, 1376, 1128, 1051, 835 cm^{-1}. EIMS: m/z 240.2 $[M + H]^+$ (2), 194.2 (3), 172.1 (2), 116.1 (4), 102.1 (100), 88.1 (5), 69.1 (8), 58.1 (61). HREIMS: m/z 238.2172 (calcd for $C_{15}H_{28}NO$ $[M - H]^+$ 238.2171).

3-[*N*-Methyl-*N*-[4,8-dimethyl-3*E*,7*E*-nonadienyl]amino]-propyl Diphosphate (3-azahomoFPP, 12). The diphosphate was prepared from amino alcohol **10b** as described above for **4b** except that the extraction buffer was 1:2:2 (v/v/v) 25 mM aqueous NH_4HCO_3/CH_3CN/2-propanol. Yield, 353 mg (80%, 93% purity by ^{31}P NMR). ^{1}H NMR (500 MHz, ND_4OD/D_2O): δ 4.93 (br d, 2 H, J = 6.9), 3.84 (t, 2 H, J = 5.8, 5.6), 3.09 (t, 2 H, J = 7.1), 2.90 (t, 2 H, J = 7.5), 2.65 (s, 3 H), 2.26 (q, 2 H, J = 7.9), 1.92−1.86 (m, 4 H), 1.84 (q, 2 H, J = 7.5), 1.47 (s, 6 H), 1.40 (s, 3 H). ^{13}C NMR (125 MHz, ND_4OD/D_2O): δ 139.9, 132.6, 124.2, 118.1, 62.9, 54.7, 53.1, 39.7, 39.0, 38.5 (d, J = 3.7), 25.9, 25.1, 24.6 (d, J = 8.3), 22.1, 17.1, 15.4. ^{31}P NMR (202 MHz, ND_4OD/D_2O): δ −7.66 (d, 1 P, J = 19.8), −9.70 (d, 1 P, J = 21.4). LRFABMS (H_2O): m/z 400.2. HRFABMS (positive ion) Calcd for $C_{15}H_{32}NO_7P_2$, 400.1654; found, 400.1652. The ^{31}P NMR spectrum showed an extra peak attributed to inorganic monophosphate [δ_P 1.44 (s, 0.07 P)].

***N*-Octylaminomethane-1,1-bisphosphonic Acid (30).** This compound was prepared by reaction of *n*-octylamine with

ethyl orthoformate and diethyl phosphite followed by hydrolysis in 6 M HCl.[10,22]

***N*-Methyl-*N*-pentyl-3-amino-1-hydroxypropane-1,1-bisphosphonic Acid (Ibandronate, 32).** The bisphosphonate was prepared by reaction of *N*-methyl-*N*-pentylamine and acrylonitrile followed by hydrolysis in 75% H_2SO_4 and reductive phosphonylation with H_3PO_3/PCl_3.[10,21] Absolute compound purities as determined from these experiments were 98.2 and 99.4% for **30** and **32**, respectively.

Inhibition of hrGGPP Synthase. The following hexahis-tagged human recombinant (hr) geranyl-geranyl diphosphate synthase (320AA)[16]—*MGSS**HHHHHH**SSGLVPRGSH*MEKT-QETVQRILLEPYKYLLQLPGKQVRTKLSQAFNHWLK-VPEDKLQIIIEVTEMLHNASLLIDDIEDNSKLRRGFPV-AHSIYGIPSVINSANYVYFLGLEKVLTLDHPDAVKLFT-RQLLELHQGQGLDIYWRDNYTCPTEEEYKAMVLQKT-GGLFGLAVGLMQLFSDYKEDLKPLLNTLGLFFQIRDD-YANLHSKEYSENKSFCEDLTEGKFSFPTIHAIW-SRPESTQVQNILRQRTENIDIKKYCVHYLEDVGS-FEYTRNTLKELEAKAYKQIDARGGNPELVALVKHL-SKMFKEENE—was used in this study. A cDNA coding for this enzyme was cloned into the *Nde*I and *Bam*HI sites of an expression vector pET-15b (Novagen). *Escherichia coli* BL21 (DE3) cells transformed with the plasmid were grown to an A_{600} of 0.6. Isopropyl 1-thio-β-D-galactopyranoside was added to a final concentration of 1 mM, and after 3 h culture, the cells were collected and suspended in 20 mM Tris-HCl buffer (pH 7.9) containing 5 mM imidazole and 500 mM NaCl. The suspensions were sonicated, and the expressed hexahis-tagged proteins were purified by nickel affinity column chromatography. The purified enzyme fractions were combined, dialyzed against Tris-HCl buffer (pH 7.9) containing 500 mM NaCl, and stored at −80 °C before use. Protein (100 ng) in 50 mM potassium phosphate buffer (pH 7.0) containing 5 mM $MgCl_2$, 2 mM DTT, 1 mg/mL BSA, and either 25 μM GPP or FPP in a total volume of 23.5 μL was incubated at 0 °C for 15 min. Then, 1.5 μL of a 0.35 mM solution of [^{14}C]IPP was added, the mixture was incubated at 37 °C for 15 min, and the pH was lowered by addition of 75 μL of HCl/MeOH to effect hydrolysis of the allylic PPs present. Following a second 15 min incubation at 37 °C, the reaction mixture was neutralized by addition of 37.5 μL of 6 N NaOH. Prenyl alcohols were then extracted with 200 μL of hexane, and a 100-μL aliquot was transferred to a scintillation vial for radioactivity counting. The quantitative activity results used in the QSAR analysis and reported in Table 1 were derived only using FPP as the substrate. The distribution of ^{14}C before acidification and hydrolysis was determined by separating IPP, GPP, FPP, and GGPP using normal phase TLC (Merck 11845 silica gel plates) using a 2-propanol/ammonia/H_2O 6:3:1 (v/v/v) solvent system (Figure 4). Spots were visualized with a Bio-image analyzer BAS1000 (Fuji Film).

3D-QSAR/CoMFA. CoMFA was performed within the QSAR module of Cerius^2 4.6 using default settings. Molecular mechanics calculations were carried out with the Cerius^2 standard universal force field, with a convergence criterion requiring a minimum energy change of 0.001 kcal/mol. Charge calculations were performed by using the Gasteiger−Marsili method.[28] CoMFA was used to evaluate the interaction energy between a probe (H^+, OH^- (donor/acceptor), and CH_3), and the molecule of interest at a series of points defined by a rectangular grid around the surface of the aligned molecules. The atomic coordinates of the models were used to compute field values on each point of the 3D grid. Grid size was adjusted to 2.00 Å. Each energy associated with an MFA grid point served as input for calculation of the QSAR results. To obtain a quantitative analysis of the dependence of biological activity on MFA parameters, regression analysis was applied, leading to the equations given in the text.

Supporting Information Available: Schemes 1 and 2 showing synthetic routes to azaprenyl diphosphates **5**−**7**, **11**, and **12** and general experimental aspects. This material is available free of charge via the Internet at http://pubs.acs.org.

Acknowledgment. This work was supported by the United States Public Health Organization (NIH Grants GM-50698 (E.O.) and GM-13956 (R.M.C.)), by the UNDP/World Bank/WHO Special Program for Research and Training in Tropical Diseases (TDR) (E.O.), and by the National Computational Science Alliance (NSF Grants MCB-000016N (E.O.), MCB-000018N (E.O.), and MCB-000020N (E.O.)). C.M.S. was supported by NIH Training Grant GM-08276. M.B.M. was an American Heart Association, Midwest Affiliate, Predoctoral Fellow.

References

(1) Jacobson, T. A.; Schein, J. R.; Williamson, A.; Ballantyne, C. M. Maximizing the Cost-Effectiveness of Lipid-Lowering Therapy. *Arch. Intern. Med.* **1998**, *158*, 1977−1989.

(2) Martin, M. B.; Arnold, W.; Heath, H. T., III; Urbina, J. A.; Oldfield, E. Nitrogen-Containing Bisphosphonates as Carbocation Transition State Analogues for Isoprenoid Biosynthesis. *Biochem. Biophys. Res. Commun.* **1999**, *263*, 754−758.

(3) Cromartie, T. H.; Fisher, K. J.; Grossman, J. N. The Discovery of a Novel Site of Action of Herbicidal Bisphosphonates. *Pestic. Biochem. Physiol.* **1999**, *63*, 114−126.

(4) Keller, R. K.; Fliesler, S. J. Mechanism of Aminobisphosphonate Action: Characterization of Alendronate Inhibition of the Isoprenoid Pathway. *Biochem. Biophys. Res. Commun.* **1999**, *266*, 560−563.

(5) Bergstrom, J. D.; Bostedor, R. G.; Masarachia, P. J.; Reszka, A. A.; Rodan, G. Alendronate is a Specific, Nanomolar Inhibitor of Farnesyl Diphosphate Synthase. *Arch. Biochem. Biophys.* **2000**, *373*, 231−241.

(6) Grove, J. E.; Brown, R. J.; Watts, D. J. The Intracellular Target for the Antiresorptive Aminobisphosphonate Drugs in *Dictyostelium discoideum* is the Enzyme Farnesyl Diphosphate Synthase. *J. Bone Miner. Res.* **2000**, *15*, 971−981.

(7) van Beek, E.; Pieterman, E.; Cohen, L.; Lowik, C.; Papapoulos, S. Farnesyl Pyrophosphate Synthase is the Molecular Target of Nitrogen-Containing Bisphosphonates. *Biochem. Biophys. Res. Commun.* **1999**, *264*, 108−111.

(8) Benford, H. L.; McGowan, N. W.; Helfrich, M. H.; Nuttall, M. E.; Rogers, M. J. Visualization of Bisphosphonate-Induced Caspase-3 Activity in Apoptotic Osteoclasts in vitro. *Bone* **2001**, *28*, 465−473.

(9) Halasy-Nagy, J. M.; Rodan, G. A.; Reszka, A. A. Inhibition of Bone Resorption by Alendronate and Risedronate does not Require Osteoclast Apotosis. *Bone* **2001**, *29*, 553−559.

(10) Martin, M. B.; Grimley, J. S.; Lewis, J. C.; Heath, H. T., III; Bailey, B. N.; Kendrick, H.; Yardley, V.; Caldera, A.; Lira, R.; Urbina, J. A.; Moreno, S. N.; Docampo, R.; Croft, S. L.; Oldfield, E. Bisphosphonates Inhibit the Growth of *Trypanosoma brucei*, *Trypanosoma cruzi*, *Leishmania donovani*, *Toxoplasma gondii*, and *Plasmodium falciparum*: a Potential Route to Chemotherapy. *J. Med. Chem.* **2001**, *44*, 909−916.

(11) Moreno, B.; Bailey, B. N.; Luo, S.; Martin, M. B.; Kuhlenschmidt, M.; Moreno, S. N. J.; Docampo, R.; Oldfield, E. ^{31}P NMR of Apicomplexans and the Effects of Risedronate on *Cryptosporidium parvum* Growth. *Biochem. Biophys. Res. Commun.* **2001**, *284*, 632−637.

(12) Yardley, V.; Khan, A. A.; Martin, M. B.; Slifer, T. R.; Araujo, F. G.; Moreno, S. N. J.; Docampo, R.; Croft, S. L.; Oldfield, E. In Vivo Activity of the Farnesyl Pyrophosphate Synthase Inhibitors Alendronate, Pamidronate and Risedronate Against *Leishmanai donovani* and *Toxoplasma gondii*. *Antimicrob. Agents Chemother.* **2002**, *46*, 929−931.

(13) Rodriguez, N.; Bailey, B. N.; Martin, M. B.; Oldfield, E.; Urbina, J. A.; Docampo, R. Unpublished results.

(14) Coxon, F. P.; Helfrich, M. H.; Van't Hof, R.; Sebti, S.; Ralston, S. H.; Hamilton, A.; Rogers, M. J. Protein Geranylgeranylation is Required for Osteoclast Formation, Function, and Survival: Inhibition by Bisphosphonates and GGTI-298. *J. Bone Miner. Res.* **2000**, *15*, 1467−1476.

(15) (a) Sagami, H.; Korenaga, T.; Ogura, K.; Steiger, A.; Pyun, H. J.; Coates, R. M. Studies on Geranylgeranyl Diphosphate Synthase from Rat Liver: Specific Inhibition by 3-Azageranylgeranyl Diphosphate. *Arch. Biochem. Biophys.* **1992**, *297*, 314−320. (b) Steiger, A.; Pyun, H.-J.; Coates, R. M. Synthesis and Characterization of Aza Analogue Inhibitors of Squalene and Geranylgeranyl Diphosphate Synthases. *J. Org. Chem.* **1992**, *57*, 3444−3449.

(16) Kuzuguchi, T.; Morita, Y.; Sagami, I.; Sagami, H.; Ogura, K. Human Geranylgeranyl Diphosphate Synthase: cDNA Cloning and Expression. *J. Biol. Chem.* **1999**, *274*, 5888−5894.

(17) (a) Koyama, T.; Ogura, K. Isopentenyl Diphosphate Isomerase and Prenyl Transferases. In *Isoprenoids Including Carotenoids and Steroids*; Cane, D. E., Ed.; Comprehensive Natural Products Chemistry; 1999; Vol. 2, Chapter 4, pp 86−96. (b) Ogura, K.; Koyama, T. Enzymatic Aspects of Isoprenoid Chain Elongation. *Chem. Rev.* **1998**, *98*, 1263−1276.

(18) *Catalyst*, version 4.6; Molecular Simulations Inc.: Burlington, MA, 2000.

(19) Meyers, A. I.; Ten Hoeve, W. α-Substitution of Amines via Dipole Stabilized Carbanions from Formamidines. *J. Am. Chem. Soc.* **1980**, *102*, 7125−7126.

(20) (a) Davisson, V. J.; Woodside, A. B.; Neal, T. R.; Stremler, K. E.; Muehlbacher, M.; Poulter, C. D. Phosphorylation and Isoprenoid Alcohols. *J. Org. Chem.* **1986**, *51*, 4768−4779. (b) Woodside, A. B.; Huang, Z.; Poulter, C. D. Trisammonium Geranyl Diphosphate. *Organic Syntheses*; Wiley and Sons: New York, 1993; Collect. Vol. VIII, p 616. (c) Davission, V. J.; Woodside, A. B.; Poulter, C. D. Synthesis of Allylic and Homoallylic Isoprenoid Pyrophosphates. *Methods Enzymol.* **1985**, *110A*, 130.

(21) Kieczykowski, G. R.; Jobson, R. B.; Melillo, D. G.; Reinhold: D. F.; Grenda, V. J.; Shinkai, I. Preparation of (4-Amino-1-Hydroxybutylidene) Bisphosphonic Acid Sodium Salt, MK-217 (Alendronate Sodium). An Improved Procedure for the Preparation of 1-Hydroxy-1,1-Bisphosphonic Acids. *J. Org. Chem.* **1995**, *60*, 8310−8312.

(22) Soloducho, J.; Gancarz, R.; Wieczorek, P.; Korf, J.; Hafner, J.; Lejczak, B.; Kafarski, P. Patent PL93-298436 93408, 1993; Chem. Abstr. No. 128:61631.

(23) Benedict, J. J.; Perkins, C. B. European Patent Application #853091403, 1995.

(24) Dunford, J. E.; Thompson, K.; Coxon, F. P.; Luckman, S. P.; Hahn, F. M.; Poulter, C. D.; Ebetino, F. H.; Rogers, M. J. Structure−Activity Relationships for Inhibition of Farnesyl Diphosphate Synthase in vitro and Inhibition of Bone Resorption in vivo by Nitrogen-Containing Bisphosphonates. *J. Pharmacol. Exp. Ther.* **2001**, *296*, 235−242.

(25) Montalvetti, A.; Bailey, B. N.; Martin, M. B.; Severin, G. W.; Oldfield, E.; Docampo, R. Bisphosphonates are Potent Inhibitors of *Trypanosoma cruzi* Farnesyl Pyrophosphate Synthase. *J. Biol. Chem.*, **2001**, *276*, 33930−33937.

(26) *Cerius*^{2} *Modeling Environment*, version 4.6; Accelrys Inc.: San Diego, CA, 2001.

(27) Tarshis, L. C.; Proteau, P. J.; Kellogg, B. A.; Sacchettini, J. C.; Poulter, C. D. Regulation of Product Chain Length by Isoprenyl Diphosphate Synthases. *Proc. Natl. Acad. Sci. U.S.A.* **1996**, *93*, 15018−15023.

(28) Gasteiger, J.; Marsili, M. Iterative Partial Equalization of Orbital Electronegativity: a Rapid Access to Atomic Charges. *Tetrahedron* **1980**, *36*, 3219−3222.

(29) Hasegawa, K.; Funatsu, K. Partial Least Squares Modeling and Genetic Algorithm Optimization in Quantitative Structure−Activity Relationships. *SAR QSAR Environ. Res.* **2000**, *11*, 189−209.

(30) Cramer, R. D.; Bunce, J. D.; Patterson, D. E.; Frank, I. E. Crossvalidation, Bootstrapping, and Partial Least Squares Compared with Multiple Regression in Conventional QSAR Studies. *Quant. Struct.-Act. Relat.* **1988**, *7*, 18−25.

(31) (a) Martin, M. B.; Kendrick, H.; de Luca-Fradley, K.; Lewis, J. C.; Grimley, J. S.; van Brussel, E. M.; Olsen, J. R.; Croft, S. L.; Oldfield, E. A Study of the Activity of Biosphosphonates Against *Trypanosoma brucei rhodesiense*: Farnesyl Pyrophosphate Synthase as a Drug Target and an Analysis of Drug Toxicity. Unpublished results. (b) Szabo, C. M.; Martin, M. B.; Oldfield, E. An Investigation of Bone Resorption and *Dictyostelium discoidium* Growth Inhibition by Bisphosphonate Drugs. Unpublished results.

(32) Sagami, H.; Morita, Y.; Ogura, K. Purification and Properties of Geranylgeranyl-Diphosphate Synthase from Bovine Brain. *J. Biol. Chem.* **1994**, *269*, 20561−20566.

(33) (a) Laskovics, F. M.; Poulter, C. D. Prenyltransferase. Determination of the Binding Mechanism and Individual Kinetic Constants for Farnesylpyrophosphate Synthase by Rapid Quench and Isotope Partitioning Experiments. *Biochemistry* **1981**, *20*, 1893−1901. (b) Mathis, J. R.; Poulter, C. D. Yeast Protein Farnesyltransferase. A Presteady-State Kinetic Analysis. *Biochemistry* **1997**, *36*, 6367−6376. (c) Poulter, C. D.; Rilling, H. C. Prenyltransferase and Isomerase. In *Biosynthesis of Isoprenoid Compounds*; Porter, J. W., Spurgenon, S. L., Eds; J. Wiley: New York, 1981; Vol. I, Chapter 4.

(34) Kaminski, J. J.; Rane, D. F.; Snow, M. E.; Weber, L.; Rothofsky, M. L.; Anderson, S. D.; Lin, S. L. Identification of Novel Farnesyl Protein Transferase Inhibitors Using Three-Dimensional Database Searching Methods. *J. Med. Chem.* **1997**, *40*, 4103−4112.

(35) Ravn, J. J.; Jin, A. Q.; Coates, R. M. Synthesis of Allylic Isoprenoid Diphosphates by S_N2 Displacement of Diethyl Phosphate. *Eur. J. Org. Chem.* **2000**, *8*, 1401−1410.

(36) Fung, A. K. L.; Baker, W. R.; Fakhoury, S.; Stein, H. H.; Cohen, J.; Donner, B. G.; Garvey, D. S.; Spina, K. P.; Rosenberg, (1α,-2β,3β,4α-1,2-Bis[*N*-propyl-*N*-(4-phenoxybenzyl)amino]carbonyl] cyclobutane-3,4-dicarboxylic Acid(A-87049): A Novel Potent Squalene Synthase Inhibitor. *J. Med. Chem.* **1997**, *40*, 2123-2125.

(37) Fieser, L. F.; Fieser, M. *Reagents for Organic Synthesis*; John Wiley & Sons: New York, 1967; pp 581−595.

(38) Ganesan, A.; Heathcock, C. H. A Stereochemical Test of the Mechanism of Electrophilic Substitution in 3-Substituted Indoles. *Tetrahedron Lett.* **1993**, *34*, 439−440.

JM010412Y